JBC ARTICLE

Analysis of autophagy activated during changes in carbon source availability in yeast cells

Received for publication, September 4, 2018, and in revised form, February 5, 2019 Published, Papers in Press, February 12, 2019, DOI 10.1074/jbc.RA118.005698

Ryo Iwama and Yoshinori Ohsumi[1]

From the Cell Biology Center, Institute of Innovative Research, Tokyo Institute of Technology, 4259-S2-12 Nagatsuta-cho, Midori-ku, Yokohama, Kanagawa 226-8503, Japan

Edited by George N. DeMartino

Autophagy is a conserved intracellular degradation system in eukaryotes. Recent studies have revealed that autophagy can be induced not only by nitrogen starvation but also by many other stimuli. However, questions persist regarding the types of conditions that induce autophagy, as well as the particular kinds of autophagy that are induced under these specific conditions. In experimental studies, abrupt nutrient changes are often used to induce autophagy. In this study, we investigated autophagy induction in batch culture on low-glucose medium, in which growth of yeast (*Saccharomyces cerevisiae*) cells is clearly reflected exclusively by carbon source state. In this medium, cells pass sequentially through three stages: glucose-utilizing, ethanol-utilizing, and ethanol-depleted phases. Using GFP cleavage assay by immunoblotting methods, fluorescence microscopy, and transmission electron microscopy ultrastructural analysis, we found that bulk autophagy and endoplasmic reticulum-phagy are induced starting at the ethanol-utilizing phase, and bulk autophagy is activated to a greater extent in the ethanol-depleted phase. Furthermore, we found that mitophagy is induced by ethanol depletion. Microautophagy occurred after glucose depletion and involved incorporation of cytosolic components and lipid droplets into the vacuolar lumen. Moreover, we observed that autophagy-deficient cells grow more slowly in the ethanol-utilizing phase and exhibit a delay in growth resumption when they are shifted to fresh medium from the ethanol-depleted phase. Our findings suggest that distinct types of autophagy are induced in yeast cells undergoing gradual changes in carbon source availability.

Autophagy is a conserved eukaryotic intracellular degradation system by which cytoplasmic components are delivered to the vacuolar (lysosomal) lumen and degraded by the vacuolar hydrolytic enzymes. During autophagy, the autophagosome, a key double-membrane structure, encloses various cellular components, including cytosolic proteins and organelles. Subsequently, the outer membrane of the autophagosome fuses with the vacuolar membrane, leading to release of the inner spherical structure, called the autophagic body, into the vacuolar lumen (1). Finally, the autophagic body disintegrates, and its contents are degraded by a variety of hydrolases. Although it was initially thought that autophagy exclusively entailed bulk engulfment of the cytoplasm, many types of autophagy that selectively degrade targets have been discovered (2). In addition, it is widely recognized that autophagy is involved in a variety of physiological processes.

The types of autophagy described above are categorized as macroautophagy. Two other types of autophagy have been described: microautophagy and chaperone-mediated autophagy (3). In microautophagy, substrates are directly enwrapped by the vacuolar membrane and delivered to the vacuolar lumen (4). In chaperone-mediated autophagy, which has been characterized in higher eukaryotes, substrates for degradation directly translocate across the lysosomal membrane. Of these three types of autophagy, macroautophagy has been studied most extensively; accordingly, hereafter we will mostly refer to macroautophagy as autophagy.

Over the past 3 decades, a number of *ATG* genes, which play important roles on autophagy, have been identified, and the functions and structures of their protein products have been studied in the yeast *Saccharomyces cerevisiae* (1, 5). Fifteen Atg proteins, Atg1–10, Atg12–14, Atg16, and Atg18, play essential roles in autophagy, and these proteins are referred to as the core machinery for membrane formation. In starvation-induced autophagy, three Atg proteins, Atg17, Atg29, and Atg31, are additionally required. Most of the components of the core machinery are assembled at the pre-autophagosomal structure (PAS)[2] in close proximity to the vacuole (6). In starvation-induced autophagy, Atg17 is required for PAS organization, suggesting that it acts as a scaffold protein (7). In contrast, in some types of selective autophagy, in which specific targets are sequestered by the autophagosome, Atg11 acts as a scaffold protein (8, 9). Selective autophagy requires receptors that are localized on targets and become landmarks for degradation: Atg19 and Atg34 for Ape1 (Cvt pathway) (10, 11); Atg32 for mitochondria (mitophagy) (12, 13); Atg36 for peroxisomes (pexophagy) (14, 15); and Atg39 and Atg40 for endoplasmic

This work was supported by JSPS KAKENHI Grants JP23000015, JP16H06375, and JP17K15245. The authors declare that they have no conflicts of interest with the contents of this article.

This article contains Figs. S1 and S2, Movies S1 and S2, and supporting Experimental procedures.

[1] To whom correspondence should be addressed: Cell Biology Center, Institute of Innovative Research, Tokyo Institute of Technology, 4259-S2-12 Nagatsuta-cho, Midori-ku, Yokohama, Kanagawa 226-8503, Japan. Tel.: 81-45-924-5113; Fax: 81-45-924-5121; E-mail: yohsumi@iri.titech.ac.jp.

[2] The abbreviations used are: PAS, pre-autophagosomal structure; BODIPY, 4,4-difluoro-1,3,5,7,8-pentamethyl-4-bora-3a,4a-diaza-*s*-indacene; ER, endoplasmic reticulum; ETC, electron transport chain; FCCP, carbonyl cyanide-*p*-trifluoromethoxyphenylhydrazone; LD, lipid droplet; ROS, reactive oxygen species; TCA, tricarboxylic acid.

reticulum (ER-phagy) (16). Although we have learned a great deal about the molecular mechanisms of autophagy, several questions remain regarding the effects of autophagy on intracellular environments. In general, autophagy plays crucial roles in ensuring the supply of amino acids under nitrogen starvation (17). However, many kinds of stimuli and starvation conditions induce autophagy (18–21). Under those conditions, autophagy plays diverse roles beyond supplying amino acids. To elucidate the physiological roles of autophagy, it is necessary to address a fundamental issue regarding autophagy: what kinds of conditions induce which kinds of autophagy?

Carbon compounds are used for energy production and as basic building blocks of cells. In eukaryotes, glycolysis in the cytosol and the tricarboxylic acid (TCA) cycle and electron transport chain (ETC) in the mitochondria play pivotal roles in energy production (22). Glucose is one of the most important carbon compounds because many organisms utilize it as a primary carbon source. In many eukaryotes, glucose is assimilated in the presence of oxygen to produce ATP through glycolysis, the TCA cycle, and the ETC. However, in the presence of oxygen the yeast *S. cerevisiae* exclusively uses glycolysis to obtain ATP from glucose (23, 24), and then it continues to produce ethanol. Therefore, if the yeast is cultured in glucose-containing medium, ethanol accumulates in the medium until the glucose is depleted. After glucose depletion, the yeast begins to use ethanol to generate ATP in the mitochondria (25). This phenomenon is referred to as the "Crabtree effect" and can be explained by glucose repression, a phenomenon in which the presence of glucose suppresses respiration, the use of alternative carbon sources, and gluconeogenesis (26). For these reasons, *S. cerevisiae* cultured in glucose-containing medium undergoes two growth phases (diauxie) separated by a period of growth arrest: during the first phase, when glucose is used, growth is rapid, whereas during the second phase, when ethanol is used, growth is slower. The growth arrest is called the "diauxic shift" (25). During the diauxic shift, the mitochondria are developed to produce ATP (27). Based on these unique features, *S. cerevisiae* is a good model organism in which to examine biological processes related to carbon source state.

In various studies, abrupt nutrient depletion has been used to induce autophagy. However, such drastic changes are not common; rather, more gradual changes are likely to occur in natural environments. Accordingly, investigation of autophagy occurring during continuous nutrient changes may lead to a better understanding of the functions of autophagy in natural habitats. In this study, we found that yeast growth in batch culture on synthetic medium with low-glucose is reflected exclusively by carbon source state. Using this medium, we investigated autophagy induction in each phase. We found that distinct cellular components are degraded via macroautophagy and microautophagy after glucose depletion. In particular, we discovered that mitophagy is induced by ethanol depletion after respiratory growth. Our findings suggest that distinct types of autophagy are induced under gradual changes of carbon source availability in yeast.

Results

In synthetic medium containing low glucose, yeast growth is reflected exclusively by carbon source availability

The yeast *S. cerevisiae* exhibits diauxie when cultured in glucose-containing medium. Although many reports have described diauxic growth in *S. cerevisiae*, there is little detailed information about the relationships among cell density, glucose, and ethanol concentration in batch culture. To investigate this issue, we cultured prototrophic WT cells (X2180-1B strain) in standard SD medium containing 0.5% casamino acids (SDCA medium) and measured those parameters in detail (Fig. 1*A*). The cells grew logarithmically while utilizing glucose and producing ethanol. When glucose was exhausted, cell proliferation was temporarily arrested, and at the same time, ethanol concentration reached a maximum. After a while, the cells restarted their growth, causing the ethanol concentration to gradually decrease. Ethanol-utilizing growth did not follow a logarithmic pattern, as reported previously (18, 28). To our surprise, ethanol was not depleted even when ethanol-utilizing growth was almost arrested. This result suggests that growth arrest is not caused by depletion of ethanol in SDCA medium, but instead by other factors.

There are at least two approaches to making yeast growth directly reflect carbon source availability: increasing the concentrations of other nutrients or decreasing glucose concentration. As shown in Fig. 1*A*, the OD_{600} reached 8–9 by the time that glucose was depleted in SDCA medium. We considered that the effects of high cell density would interfere with yeast growth in the ethanol-utilizing phase even if we increased the levels of other nutrients in SDCA medium. To avoid those effects, we lowered the glucose concentration. When we cultured WT cells in synthetic medium containing 0.2% glucose and 0.5% casamino acids ($SD_{0.2}CA$ medium), the cells temporarily stopped their growth at an OD_{600} of ~1.2 (Fig. 1*B*). After the growth arrest, the cells restarted their growth by using ethanol. In contrast to the growth pattern in SDCA medium, ethanol-utilizing growth was logarithmic in $SD_{0.2}CA$ medium (Fig. 1*D*). During growth, the oxygen consumption rate was higher in $SD_{0.2}CA$ medium than in SDCA medium in the absence or presence of FCCP, an uncoupling reagent, suggesting that respiratory potential is higher in $SD_{0.2}CA$ medium than in SDCA medium (Fig. 1*C*). Importantly, arrest of ethanol-utilizing growth in $SD_{0.2}CA$ medium occurred at the time when ethanol was exhausted. Furthermore, we confirmed that the yeast did not show significant growth on SCA medium, which did not contain glucose, in our experimental duration (Fig. S1*A*). Because OD_{600} exceeds 10 in SDCA medium, we considered that nitrogen sources are enough for yeast growth in $SD_{0.2}CA$ medium. As expected, ammonium was not depleted during cultivation, and extra ammonium did not improve the yeast growth (Fig. S1, *B* and *C*). Therefore, we concluded that $SD_{0.2}CA$ is a suitable model medium in which yeast growth is reflected exclusively by carbon source availability. In $SD_{0.2}CA$ medium, three stages of yeast growth became obvious: glucose-utilizing, ethanol-utilizing, and ethanol-depleted (stationary) phases (Fig. 1*E*). Hereafter, we primarily used $SD_{0.2}CA$ medium to analyze the effects of carbon source availability.

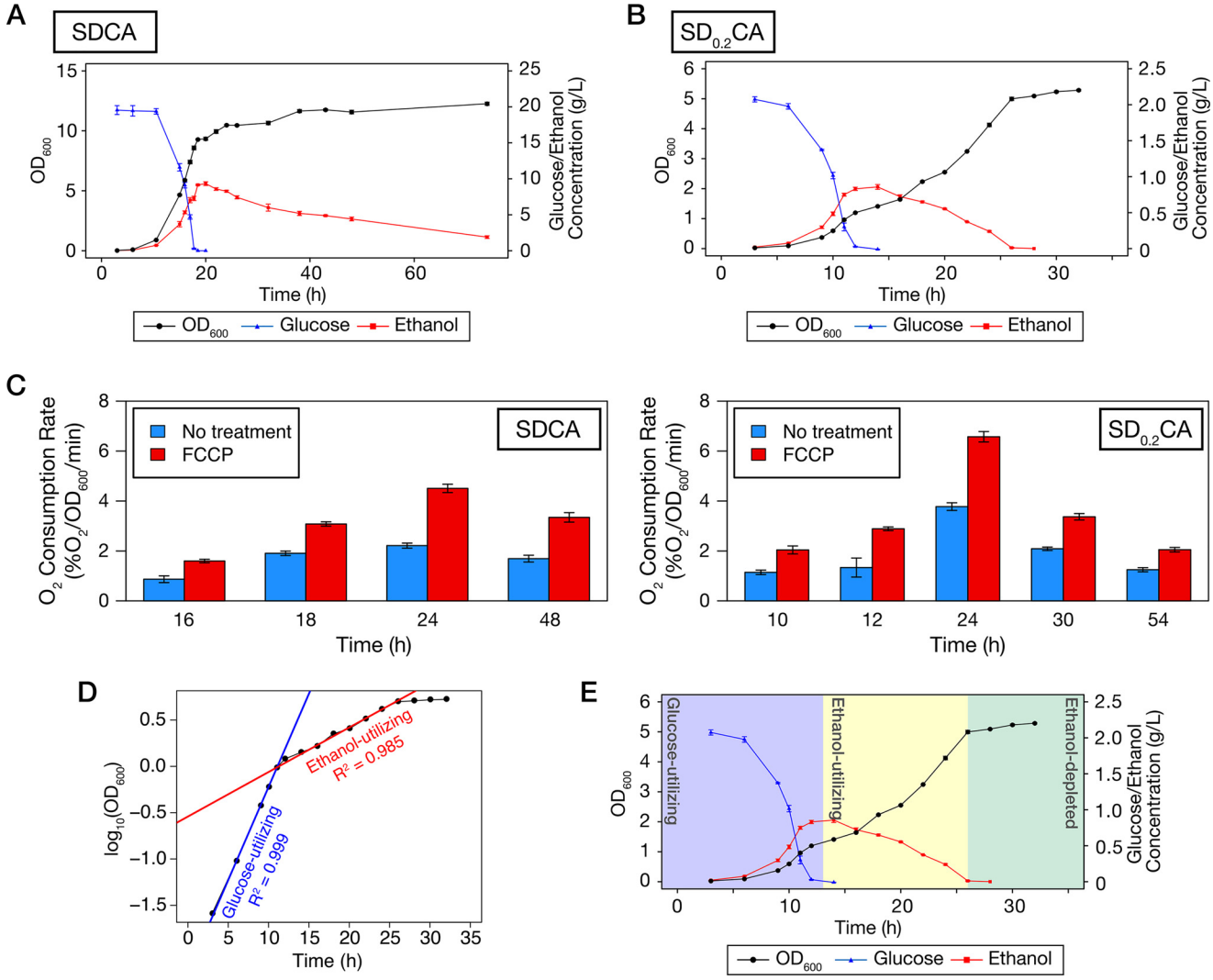

Figure 1. Yeast cells undergo three distinct growth stages in low-glucose medium. *A* and *B*, prototrophic WT cells were inoculated into SDCA (*A*) or $SD_{0.2}CA$ (*B*) medium at a starting OD_{600} of 0.01 and then cultured for 74 or 32 h, respectively. OD_{600} (*black circle*), glucose concentration (*blue triangle*), and ethanol concentration (*red square*) were measured at the indicated time points. *Data points* and *error bars* indicate means ± S.E. ($n = 3$). *C*, WT cells were inoculated into SDCA medium or $SD_{0.2}CA$ medium and cultured for the indicated time periods. Cells were collected, and oxygen consumption rates were measured. Each *bar* represents mean ± S.E. ($n = 3$). *D*, growth curve in *B* is shown on a semilogarithmic graph. Regression lines and their adjusted R^2 values were calculated using data from 6 to 11 h (glucose-utilizing phase) or from 16 to 24 h (ethanol-utilizing phase). *E*, plots of OD_{600}, glucose, and ethanol concentration depicted here are derived from *B*. Yeast growth is categorized into three stages: *glucose-utilizing*, *ethanol-utilizing*, and *ethanol-depleted* phases.

Autophagy is induced after glucose depletion

We examined induction of autophagy during growth in low-glucose medium using GFP-Atg8–expressing cells. When autophagy is induced, GFP-Atg8 is delivered to the vacuolar lumen via the autophagic pathway; the GFP moiety is released from GFP-Atg8 by vacuolar proteases, and free GFP is detected by immunoblot analysis (29). Endogenous expression of GFP-Atg8 did not alter the growth features observed in WT cells cultured in low-glucose medium (data not shown). We found that cleavage of GFP-Atg8 occurred in the ethanol-utilizing and ethanol-depleted phases but not in the glucose-utilizing phase (Fig. 2*A*). The cleavage depended strongly on *ATG2* (Fig. 2*A*). In addition, we confirmed that GFP-Atg8 was delivered to the vacuolar lumen in WT but not *atg2*Δ cells (Fig. 2*B*). In a deletion mutant of *ATG15*, which encodes a putative lipase responsible for disintegration of autophagic bodies (30), we observed autophagic bodies moving around randomly (Movie S1). These autophagic bodies were not observed when *ATG2* was simultaneously deleted (Movie S1). These results indicate that autophagy is induced after glucose depletion, *i.e.* in the ethanol-utilizing and ethanol-depleted phases. Moreover, our findings suggest that autophagy is activated to a greater extent in the ethanol-depleted phase than the ethanol-utilizing phase (Fig. 2*A*).

Cytosolic components, ER, and mitochondria are degraded via autophagy

Next, we sought to determine which substrates are degraded during growth in low-glucose medium. We performed the cleavage assay using WT cells expressing Pgk1-GFP (a cytosolic protein), Sec63-GFP (an ER membrane protein), Om45-GFP (a mitochondrial outer membrane protein), Pex11-GFP (a peroxisome membrane protein), or Osw5-GFP (a lipid droplet (LD) protein). Cells were collected from each culture at the indicated

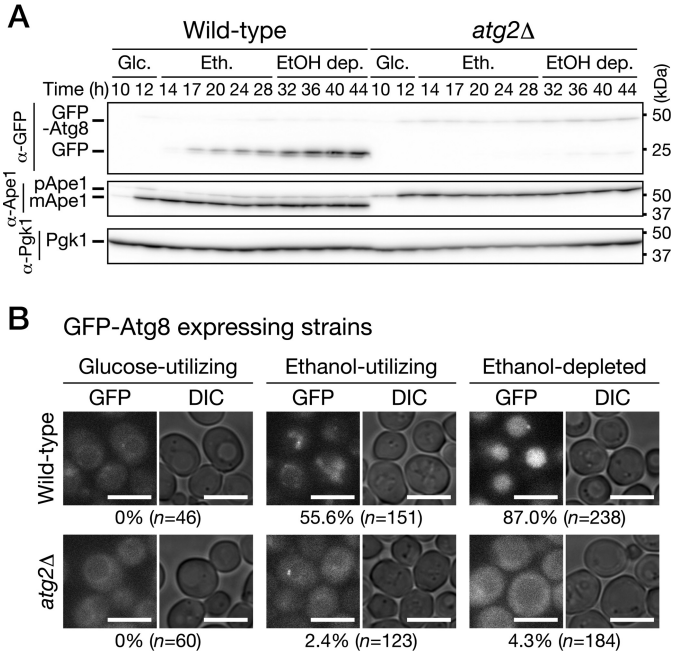

Figure 2. Autophagy is induced after glucose depletion in low-glucose medium. *A,* WT and *atg2*Δ cells expressing GFP-Atg8 were inoculated into $SD_{0.2}$CA medium at a starting OD_{600} of 0.01 and then cultured for 44 h. Cells were collected at the indicated time points and subjected to immunoblot analysis. *Glc.*, glucose-utilizing phase; *Eth.,* ethanol-utilizing phase; *EtOH dep.*, ethanol-depleted phase. *pApe1*, precursor Ape1; *mApe1*, mature Ape1. *B,* WT and *atg2*Δ cells expressing GFP-Atg8 were inoculated into $SD_{0.2}$CA medium at a starting OD_{600} of 0.01 and cultured for 10 h (*glucose-utilizing*), 22 h (*ethanol-utilizing*), or 46 h (*ethanol-depleted*). The cells were observed under a fluorescence microscope. *Bars,* 5 μm. The cells having the vacuoles with fluorescence signal were counted, and the ratio is shown. *DIC*, differential interference contrast.

time points (Fig. 3*A*), and cell lysates were subjected to immunoblot analysis using anti-GFP antibodies (Fig. 3, *B–F*). The cytosol started to be degraded in the ethanol-utilizing phase, and its rate of degradation increased in the ethanol-depleted phase (Fig. 3*B*). A similar pattern was observed in the ER degradation, although the degradation rate was very low (Fig. 3*C*). On the contrary, the mitochondria were degraded only in the ethanol-depleted phase (Fig. 3*D*). In contrast to these organelles, degradation of peroxisomes and LDs was not detected during the experiment period (total cultivation time, 100 h) (Fig. 3, *E* and *F*). Rather, the amount of Pex11-GFP increased during the ethanol-utilizing and the ethanol-depleted phases, and Osw5-GFP increased during the ethanol-utilizing phase. We ascertained that Sec63-GFP and Om45-GFP were delivered to the vacuolar lumen (Fig. 3*G*), suggesting that the ER and mitochondria are degraded in the vacuole. Electron microscopic observation of *atg15*Δ cells confirmed that the cytosol, ER, and mitochondria were incorporated into autophagic bodies (Fig. 3*H*).

To determine whether autophagy was involved in the degradation of these organelles, we cultured autophagy-defective mutants expressing Pgk1-GFP, Sec63-GFP, or Om45-GFP in $SD_{0.2}$CA medium, lysed the cells, and performed the cleavage assay on these lysates (Fig. 4). Cytosolic components, ER, and mitochondria were not degraded in cells lacking *ATG2*, suggesting that these cellular components are degraded by the autophagic pathway. Degradation of the cytosol was highly dependent on *ATG17*, but not *ATG11* (Fig. 4*A*). A similar pattern was observed for degradation of the ER (Fig. 4*B*). These results suggest that cytosolic components and the ER are degraded in an Atg17-dependent manner under our experimental condition. Importantly, double-deletion of *ATG39* and *ATG40* diminished ER degradation (Fig. 4*B*), suggesting that ER-phagy receptors are required for ER degradation under these conditions. In contrast, degradation of the mitochondria was highly dependent on *ATG11* but only partially dependent on *ATG17* (Fig. 4*C*). In addition, mitochondrial degradation was not detected in cells lacking *ATG32* (Fig. 4*C*). These results indicate that mitophagy occurs in the ethanol-depleted phase. In summary, bulk autophagy and ER-phagy were induced after glucose depletion, whereas mitophagy was induced in the ethanol-depleted phase. The possible roles of Atg17 and Atg11 are discussed below (see "Discussion").

Low-glucose medium sheds light on mitophagy during ethanol-depleted condition

Our findings suggest that autophagy is activated to a greater extent in the ethanol-depleted phase in $SD_{0.2}$CA medium (Fig. 2*A*). Consistent with this, the degradation rates of cytosolic components and the ER were higher in the ethanol-depleted phase than in the ethanol-utilizing phase (Fig. 3, *B* and *C*). The mitochondria were targets of autophagy during the ethanol-depleted phase (Fig. 3*D*). However, mitochondrial degradation was not observed during prolonged cultivation in SDCA medium (Fig. 5), suggesting that the mitochondrial degradation is induced not by long-term cultivation, but rather by ethanol depletion. It has been reported so far that mitophagy can be induced by prolonged cultivation on a nonfermentable carbon source or by shifting from a nonfermentable carbon source to nitrogen starvation medium containing glucose (12, 13, 31). In addition to those conditions, we propose that mitophagy is also induced by ethanol depletion after ethanol-utilizing growth.

Presence of amino acids may sustain autophagy activity during ethanol-depleted condition

The prototrophic WT yeast cells can synthesize the amino acids required for growth by themselves. However, as described above, we used medium containing casamino acids, acid hydrolysate of casein, to support the yeast growth. To evaluate effects of the presence of amino acids, we used low-glucose medium without casamino acids ($SD_{0.2}$ medium). Growth feature in $SD_{0.2}$ medium was similar to that in $SD_{0.2}$CA medium; yeast growth is correlated with concentration of glucose and ethanol (Fig. 6*A*). However, there were two different aspects between those two conditions. In $SD_{0.2}$ medium, the yeast growth was slower (Figs. 1*B* and 6*A*), and biomass was accumulated less in the ethanol-depleted phase (Fig. 6*B*), indicating that amino acids are used in the prototrophic yeast.

Using $SD_{0.2}$ medium, in which ammonium was not depleted during cultivation (Fig. 6*C*), we repeated GFP cleavage assay of GFP-Atg8, Pgk1-GFP, Sec63-GFP, and Om45-GFP (Fig. 6, *D–G*). Regarding time points when autophagy is induced, results similar to $SD_{0.2}$CA medium were obtained; bulk autophagy and ER-phagy were induced after glucose depletion, and mitophagy was induced in ethanol-depleted phase. We also

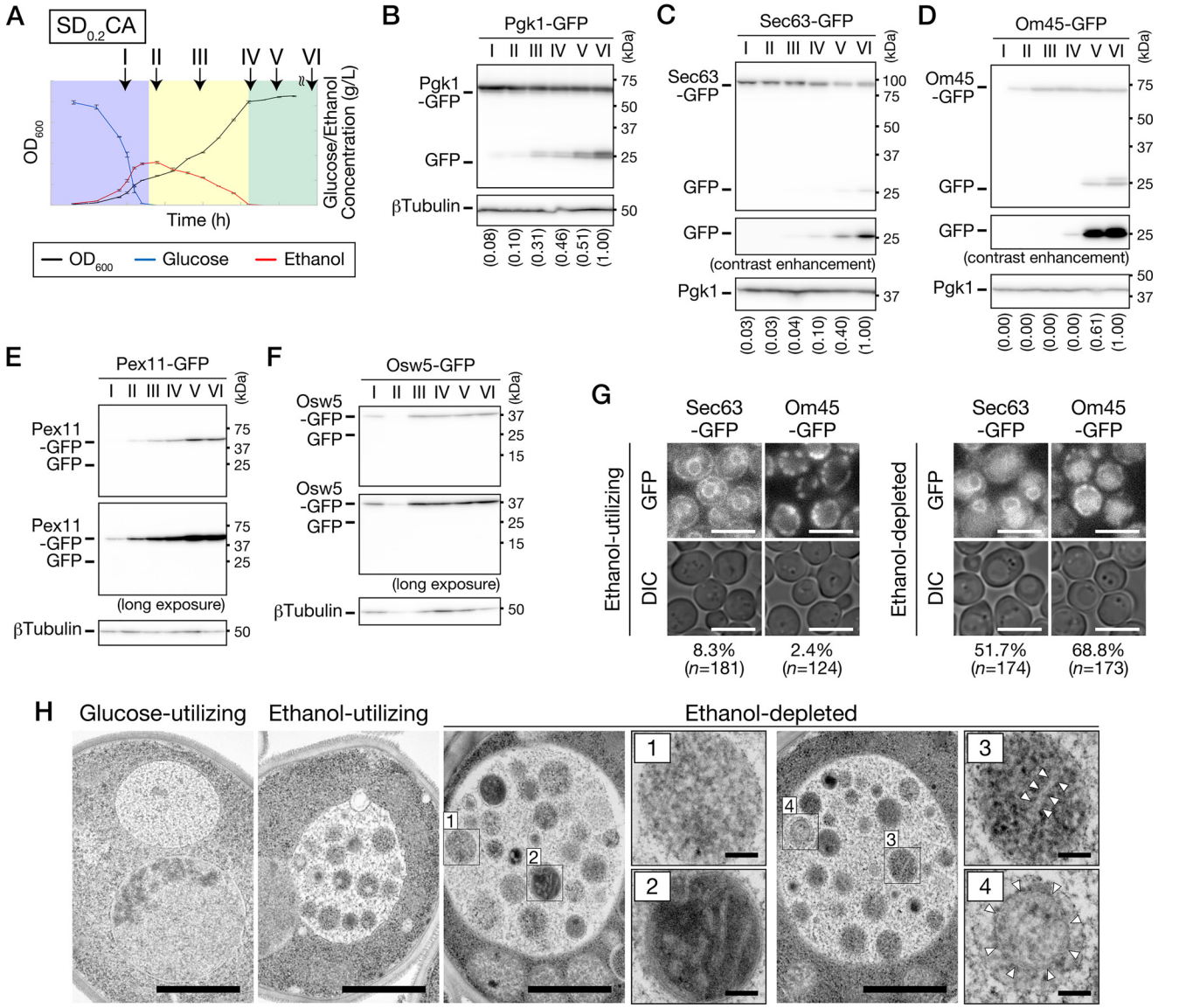

Figure 3. Cytosolic components, ER, and mitochondria are degraded during growth in low-glucose medium. *A,* time points used in Fig. 3. Plots of OD_{600}, glucose, and ethanol concentration depicted here are derived from Fig. 1*B*. *Time I*, glucose-utilizing phase (9–11 h); *time II*, early ethanol-utilizing phase (12–14 h); *time III*, middle ethanol-utilizing phase (20–24 h); *time IV*, just after ethanol depletion (26–28 h); *time V*, ethanol-depleted for 1 day (48–52 h); *time VI*, ethanol-depleted for 3 days (96–100 h). *B–F,* WT cells expressing Pgk1-GFP (*B*), Sec63-GFP (*C*), Om45-GFP (*D*), Pex11-GFP (*E*), or Osw5-GFP (*F*) were inoculated into $SD_{0.2}$CA medium at a starting OD_{600} of 0.01, cultured for 100 h, and collected at the time points indicated in *A*. Lysates from these cells were subjected to immunoblot analysis. *B–D*, intensity of each band was quantified, and GFP ratio (free GFP/β-tubulin or free GFP/Pgk1) was calculated. The values in *parentheses* are relative values to the GFP ratio of time VI. *G,* WT cells expressing Sec63-GFP or Om45-GFP were inoculated into $SD_{0.2}$CA medium at a starting OD_{600} of 0.01 and cultured for 24 h (*ethanol-utilizing*) or 48 h (*ethanol-depleted*). The cells were observed under a fluorescence microscope. *Bars,* 5 μm. The cells having the vacuoles with fluorescence signal were counted, and the ratio is shown. *DIC*, differential interference contrast. *H, atg15*Δ cells were inoculated into $SD_{0.2}$CA medium. Cells were collected in the glucose-utilizing, ethanol-utilizing, or ethanol-depleted phase and then observed by transmission EM. In the ethanol-depleted phase, autophagic bodies are shown at high magnification. *Panel 1*, cytosol; *panel 2*, mitochondrion; *panel 3*, tubule/sheet ER; *panel 4*, double-ring ER. *Arrowheads* indicate the ER membrane. *Bars,* 1 μm (lower magnification) and 100 nm (higher magnification).

ascertained that the degradation was dependent on *ATG2*. However, we noticed that some different points were observed in the ethanol-depleted phase between $SD_{0.2}$CA medium and $SD_{0.2}$ medium. In $SD_{0.2}$CA medium, the longer the ethanol-depleted phase was, the greater the amount of free GFP accumulated (Fig. 3, *B–D*). In contrast, in $SD_{0.2}$ medium, such accumulation was not observed (Fig. 6, *E–G*). In particular, ER degradation was reduced in the ethanol-depleted phase (Fig. 6*F*). It should be noted that the GFP cleavage assay only gives an indication of the amount of free GFP moieties in vacuoles at a certain time, which is determined by both influx from autophagy and degradation by vacuolar hydrolytic enzymes. Therefore, it cannot be reliably used as a quantitative measure to analyze or discuss data obtained under different conditions. Nevertheless, the results described above raised a possibility that the presence of amino acids may sustain autophagy activity during the ethanol-depleted phase.

Microautophagy occurs in the ethanol-utilizing and ethanol-depleted phases

As described above, it is considered that cleavage of GFP-Atg8 is not observed in autophagy-defective mutants. However,

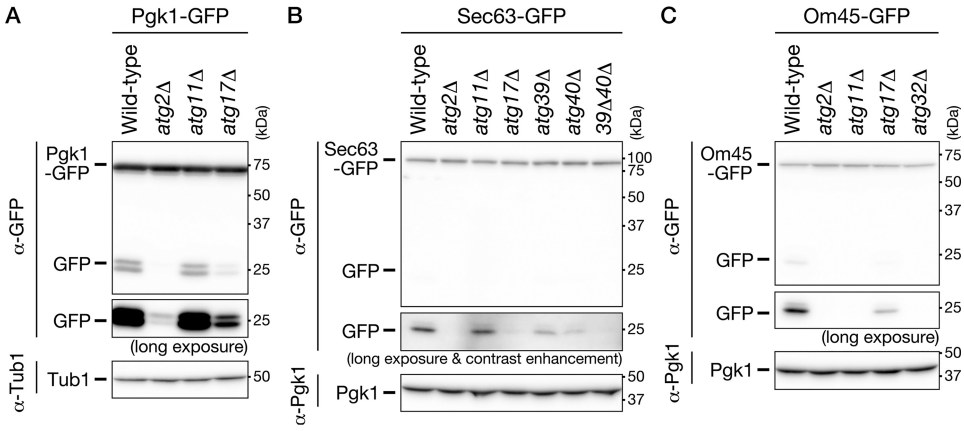

Figure 4. Cytosolic components, ER, and mitochondria are degraded via autophagic pathways under ethanol-depleted conditions. The indicated strains were inoculated into $SD_{0.2}CA$ medium at a starting OD_{600} of 0.01, and then cultured for 52 h. Cell lysates from these cells were subjected to immunoblot analysis. Strains used were as follows: WT, *atg2*Δ, *atg11*Δ, and *atg17*Δ cells expressing Pgk1-GFP (*A*); WT, *atg2*Δ, *atg11*Δ, *atg17*Δ, *atg39*Δ, *atg40*Δ, and *atg39*Δ*atg40*Δ (*39*Δ*40*Δ) cells expressing Sec63-GFP (*B*); WT, *atg2*Δ, *atg11*Δ, *atg17*Δ, and *atg32*Δ cells expressing Om45-GFP (*C*). *Tub1*, β-tubulin.

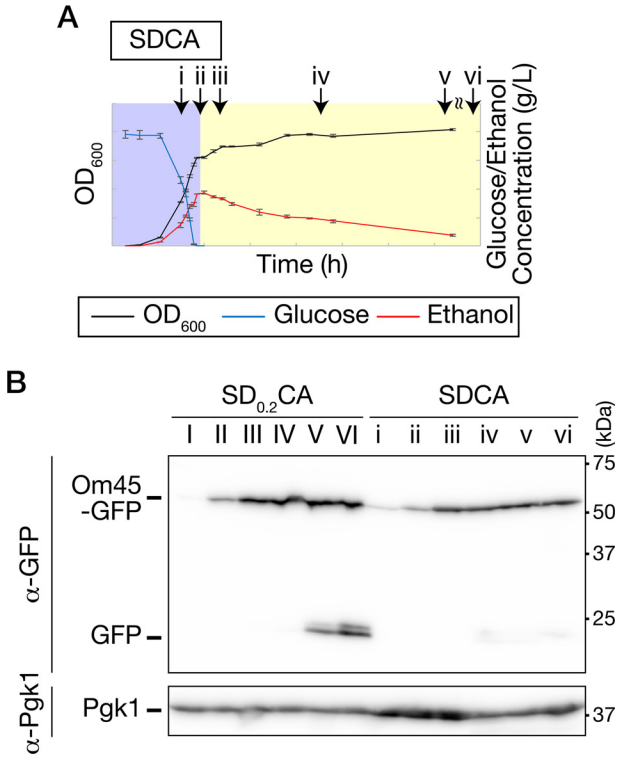

Figure 5. Mitophagy is induced under ethanol-depleted conditions after respiratory growth. *A,* time points used in *B*. Plots of OD_{600}, glucose, and ethanol concentration depicted here are derived from Fig. 1*A*. *Time i,* glucose-utilizing phase (16 h); *time ii,* early ethanol-utilizing phase (18 h); *time iii,* middle ethanol-utilizing phase (24 h); *times iv–vi,* growth arrest after respiratory growth (*iv*, 49 h; *v*, 72 h; and *vi*, 120 h). *B,* WT cells expressing Om45-GFP were inoculated into $SD_{0.2}CA$ or SDCA medium at a starting OD_{600} of 0.01 and then collected at the time points indicated in Fig. 3*A* ($SD_{0.2}CA$) or Fig. 5*A* (SDCA). Lysates from these cells were subjected to immunoblot analysis.

we detected a significant amount of free GFP, even in *atg2*Δ cells expressing GFP-Atg8, in both the ethanol-utilizing and ethanol-depleted phases (Fig. 2*A*). Hence, we investigated how cleavage of GFP-Atg8 occurred in *atg2*Δ cells.

Initially, we sought to determine whether the GFP-Atg8 cleavage occurred in deletion mutants of the other core *ATG* genes in the ethanol-depleted phase (Fig. 7*A*). GFP-Atg8 cleavage was hardly detected in single deletion mutants of *ATG3*, *ATG4*, *ATG5*, *ATG7*, *ATG10*, *ATG12*, and *ATG16*, which encode components of the ATG conjugation system. In contrast, free GFP was clearly detected in single deletion mutants of *ATG1*, *ATG2*, *ATG9*, *ATG13*, *ATG14*, and *ATG18*. Because all components of the ATG conjugation system are required for the GFP-Atg8 cleavage, this result suggests that lipidation of Atg8 is essential for its delivery to the vacuolar lumen. Therefore, assuming that the amount of GFP-Atg8 that binds to the vacuolar membrane increases when GFP-Atg8 is lipidated, we speculated that lipidated GFP-Atg8 moieties are internalized into the vacuolar lumen via microautophagy, because it is reported that microautophagy occurs after the diauxic shift in YEPD medium (32). Consistent with this idea, we found that the free GFP bands detected in *atg2*Δ cells disappeared upon simultaneous deletion of *VPS4* (Fig. 7*B*), which is involved in microautophagy after the diauxic shift (32). Furthermore, we demonstrated that cleavage of Vph1-GFP, a vacuolar membrane protein thought to be cleaved by microautophagy, occurred in the ethanol-utilizing and ethanol-depleted phases (Fig. 7*D*) and that this cleavage took place independently of the *ATG* genes (Fig. 7*C*). These results indicate that microautophagy occurs in the ethanol-utilizing and ethanol-depleted phases. On the basis of these findings, we propose that microautophagy degrades lipidated GFP-Atg8 without machineries for macroautophagy and that this is the reason that GFP-Atg8 was cleaved in *atg2*Δ cells. However, the possibility that lipidated GFP-Atg8 is transported into the vacuolar lumen via the multivesicular body pathway (33) cannot be excluded. As shown in Fig. 7*A*, we also found that cleavage of GFP-Atg8 was barely detectable in the deletion mutant of *ATG6*, which encodes a component of the phosphatidylinositol 3-kinase complex; however, the underlying reason remains to be elucidated.

Next, we performed electron-microscopic analysis to observe in detail WT cells in the glucose-utilizing and ethanol-depleted phases (Fig. 7*E*, *upper panel*). We observed spherical bodies, which we hereafter call microautophagic bodies, in the vacuolar lumen of cells in the ethanol-depleted phase; these bodies contained cytosolic components and LDs. We then confirmed, by BODIPY staining, that LDs were delivered to the

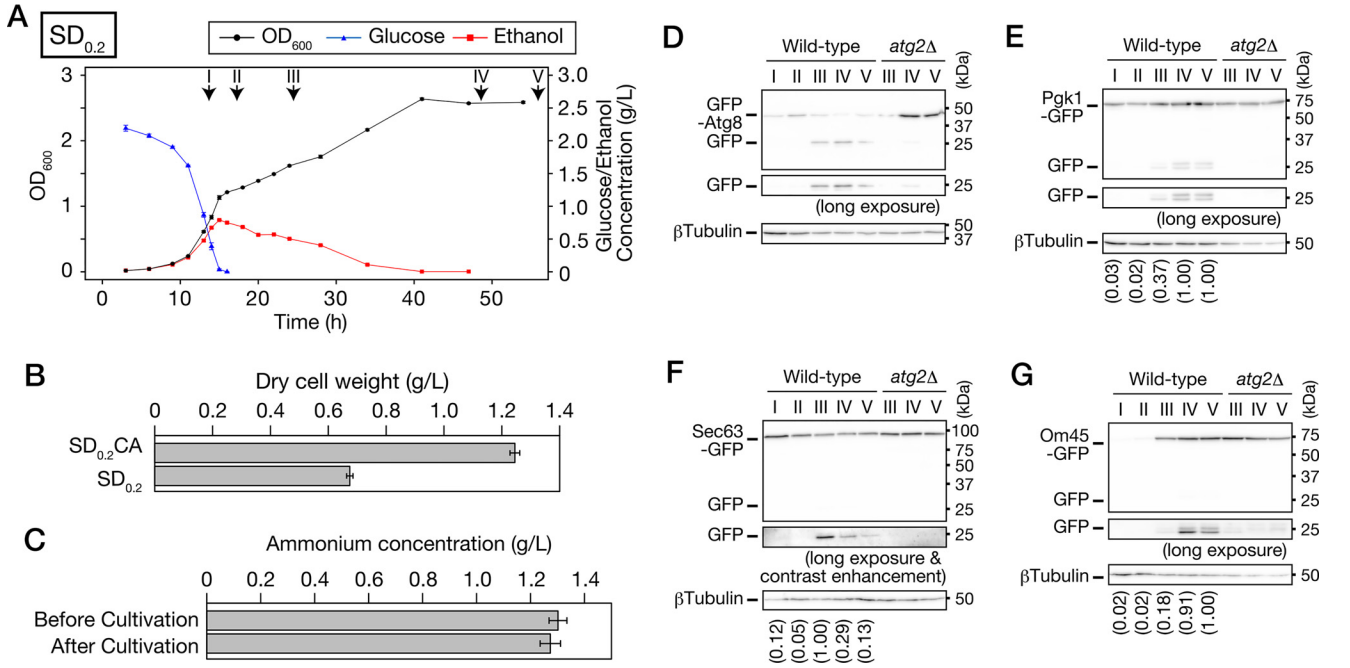

Figure 6. Cytosolic components, ER, and mitochondria are degraded via autophagy during growth in low-glucose medium without casamino acids. *A,* prototrophic WT cells were inoculated into $SD_{0.2}$ medium at a starting OD_{600} of 0.01, and then cultured for 55 h. OD_{600} (*black circle*), glucose concentration (*blue triangle*), and ethanol concentration (*red square*) were measured at the indicated time points. *Data points* and *error bars* indicate means ± S.E. ($n = 3$). Time points used in *D–G* are as follows: *I*, glucose-utilizing, 14 h; *II*, diauxic shift, 17 h; *III*, ethanol-utilizing, 24 h; *IV*, ethanol-depleted, 48 h; *V*, ethanol-depleted, 65 h. *B,* WT cells were inoculated into $SD_{0.2}$CA or $SD_{0.2}$ medium at a starting OD_{600} of 0.01 and then cultured for 48 h. Dry cell weight of yeast cells per 1 liter of culture was measured. Each *bar* represents mean ± S.E. ($n = 8$). *C,* ammonium concentration of the $SD_{0.2}$ medium before or after cultivation was measured. WT cells were inoculated into $SD_{0.2}$ medium at a starting OD_{600} of 0.01 and cultured for 48 h. The supernatant was obtained by centrifuging the culture, and ammonium concentration was measured in the supernatant. Each *bar* represents mean ± S.E. ($n = 3$). *D–G,* WT or *atg2*Δ cells expressing GFP-Atg8 (*D*), Pgk1-GFP (*E*), Sec63-GFP (*F*), or Om45-GFP (*G*) were inoculated into $SD_{0.2}$ medium at a starting OD_{600} of 0.01, cultured for 65 h, and collected at the indicated time points. Lysates from these cells were subjected to immunoblot analysis. *E–G,* intensity of each band was quantified, and GFP ratio (free GFP/β-tubulin) was calculated. The values in *parentheses* are relative values to the GFP ratio of time V (Pgk1-GFP and Om45-GFP) or time III (Sec63-GFP).

vacuolar lumen (Fig. 7*F* and Movie S2). In the ethanol-utilizing phase, it was often observed that the vacuolar membrane was directly enwrapping LD (Fig. S2). Microautophagic bodies containing the cytosol and/or LDs were also observed in the *atg2*Δ mutant (Fig. 7*E*, *lower panel*), consistent with the idea that microautophagy occurs without machineries for macroautophagy under our experimental condition. One discrepancy is that cleavage of Osw5-GFP was not detected despite incorporation of LDs into the vacuoles (Figs. 3*F* and 7, *E* and *F*). However, because disintegration of microautophagic bodies, whose membranes are derived from the vacuolar membrane, progresses very slowly, this cleavage may not be detectable.

Roles of autophagy in the ethanol-utilizing and ethanol-depleted phases

Because autophagy is induced after glucose depletion in low-glucose medium, we investigated the roles of the autophagy in growth. First, we cultured WT or *atg2*Δ cells in low-glucose medium and measured cell density, glucose, and ethanol concentration (Fig. 8*A*). In the ethanol-utilizing phase, growth and ethanol consumption rate were significantly slower in *atg2*Δ cells than in WT cells. Second, we measured the viabilities of WT and *atg2*Δ cells in the ethanol-depleted phase by phloxine B staining (Fig. 8*B*). The viabilities of these strains did not differ until 5 days after entry into the ethanol-depleted phase. Subsequently, we re-inoculated WT or *atg2*Δ cells in the ethanol-depleted phase into fresh $SD_{0.2}$CA medium, and we then measured cell density of the cultures every 10 min using an automatically recording incubator (Fig. 8*C*). In WT cells, the length of lag phase barely changed until 3 days after entry into the ethanol-depleted phase, whereas in *atg2*Δ cells, the lag phase became longer as the ethanol-depleted phase became longer. This result suggests that autophagy in the ethanol-depleted phase is required to promote re-growth in fresh medium.

Above, we demonstrated that mitophagy was induced only in the ethanol-depleted phase. Finally, we investigated whether mitophagy was required for promotion of re-growth in fresh medium (Fig. 8*D*). The *atg32*Δ strain, a mitophagy-deficient strain, exhibited delayed re-growth compared with the WT strain when it was shifted to fresh medium on day 0 or day 4 of cultivation after entry into the ethanol-depleted phase. This observation suggests that mitochondrial quality and/or quantity control in the ethanol-depleted phase is important for subsequent re-growth. However, the ER-phagy–deficient *atg39*Δ*atg40*Δ strain did not exhibit delayed re-growth. In light of the difference between *atg2*Δ and *atg32*Δ cells, this finding suggests that not only mitochondria but also other cellular components must be degraded for cells to undergo subsequent growth. Future work should seek to identify the autophagic targets that influence the ability to re-initiate growth.

Discussion

In natural environments, nutrient conditions change from moment to moment. Yeasts must adapt to these gradual

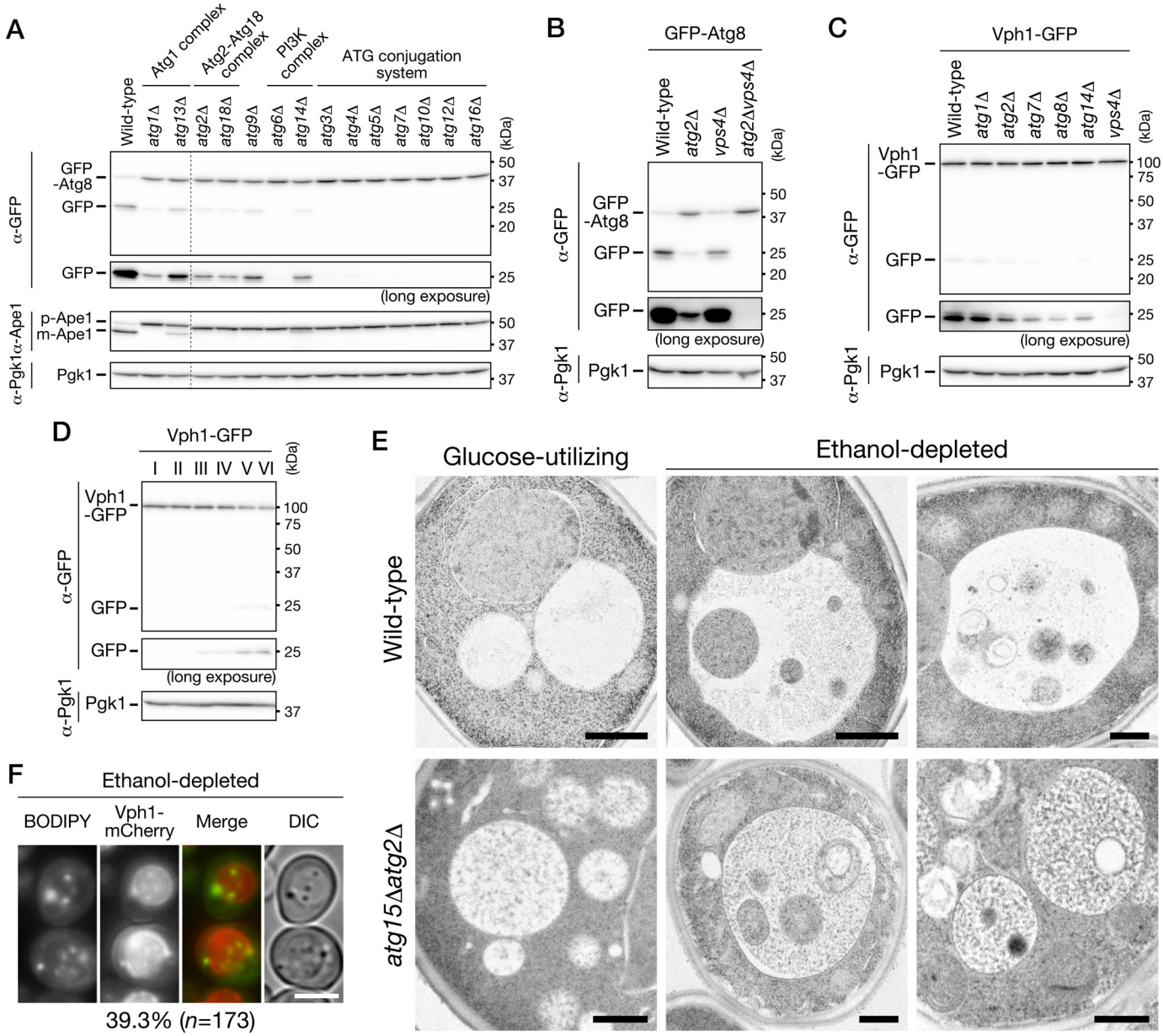

Figure 7. Microautophagy incorporates cytosol and LDs into the vacuolar lumen. *A,* WT, *atg1*Δ, *atg2*Δ, *atg3*Δ, *atg4*Δ, *atg5*Δ, *atg6*Δ, *atg7*Δ, *atg9*Δ, *atg10*Δ, *atg12*Δ, *atg13*Δ, *atg14*Δ, *atg16*Δ, or *atg18*Δ cells expressing GFP-Atg8 were inoculated into $SD_{0.2}CA$ medium at a starting OD_{600} of 0.01 and cultured for 2 days. Cell extracts were prepared from these cells and subjected to immunoblot analysis. *pApe1,* precursor Ape1; *mApe1,* mature Ape1. *B,* WT, *atg2*Δ, *vps4*Δ, and *atg2*Δ*vps4*Δ cells expressing GFP-Atg8 were inoculated into $SD_{0.2}CA$ medium at a starting OD_{600} of 0.01 and cultured for 2 days. Lysates from these cells were subjected to immunoblot analysis. *C,* WT, *atg1*Δ, *atg2*Δ, *atg7*Δ, *atg8*Δ, *atg14*Δ, and *vps4*Δ cells expressing Vph1-GFP were inoculated into $SD_{0.2}CA$ medium at a starting OD_{600} of 0.01 and cultured for 2 days. Lysates from these cells were subjected to immunoblot analysis. *D,* WT cells expressing Vph1-GFP were inoculated into $SD_{0.2}CA$ medium at a starting OD_{600} of 0.01, cultured for 100 h, and collected at the time points indicated in Fig. 3*A*. Lysates from these cells were subjected to immunoblot analysis. *E,* WT or *atg15*Δ*atg2*Δ cells were cultured for 8 h (*left*, *glucose-utilizing*) or 52 h (*middle* and *right*, *ethanol-depleted*) in $SD_{0.2}CA$ medium. Images were acquired by transmission EM. *Bars,* 500 nm. *F,* cells expressing Vph1-mCherry were cultured for 48 h in $SD_{0.2}CA$ medium. Cells were stained with BODIPY and observed by fluorescence microscopy. *Bars,* 5 μm. The cells having vacuoles that includes moving BODIPY-dots were counted, and the ratio is shown.

changes, and their growth is influenced by the availability of nutrients at that moment. Abrupt nutrient changes are often used to investigate cellular responses. In nature, however, nutrient changes are more likely to be gradual in most cases. Therefore, it is important to investigate cellular responses based on their growth along with nutrient changes.

Here, we found that carbon source availability is an important determinant of growth when yeast is cultured in $SD_{0.2}CA$ medium (Fig. 1*B*). Amino acids derived from the hydrolysate of casein contributed yeast biomass (Fig. 5*B*), but yeast growth was correlated with glucose and ethanol concentrations (Figs. 1*B* and 5*A*). We consider that casamino acids should be utilized for protein synthesis or others even in the prototrophic yeast used in this study, and that glucose and ethanol are important factors for growth state. Hence, we categorized the yeast growth in $SD_{0.2}CA$ or $SD_{0.2}$ medium into three stages: the glucose-utilizing, ethanol-utilizing, and ethanol-depleted phases (Fig. 1*E*). We investigated autophagy in each phase and found

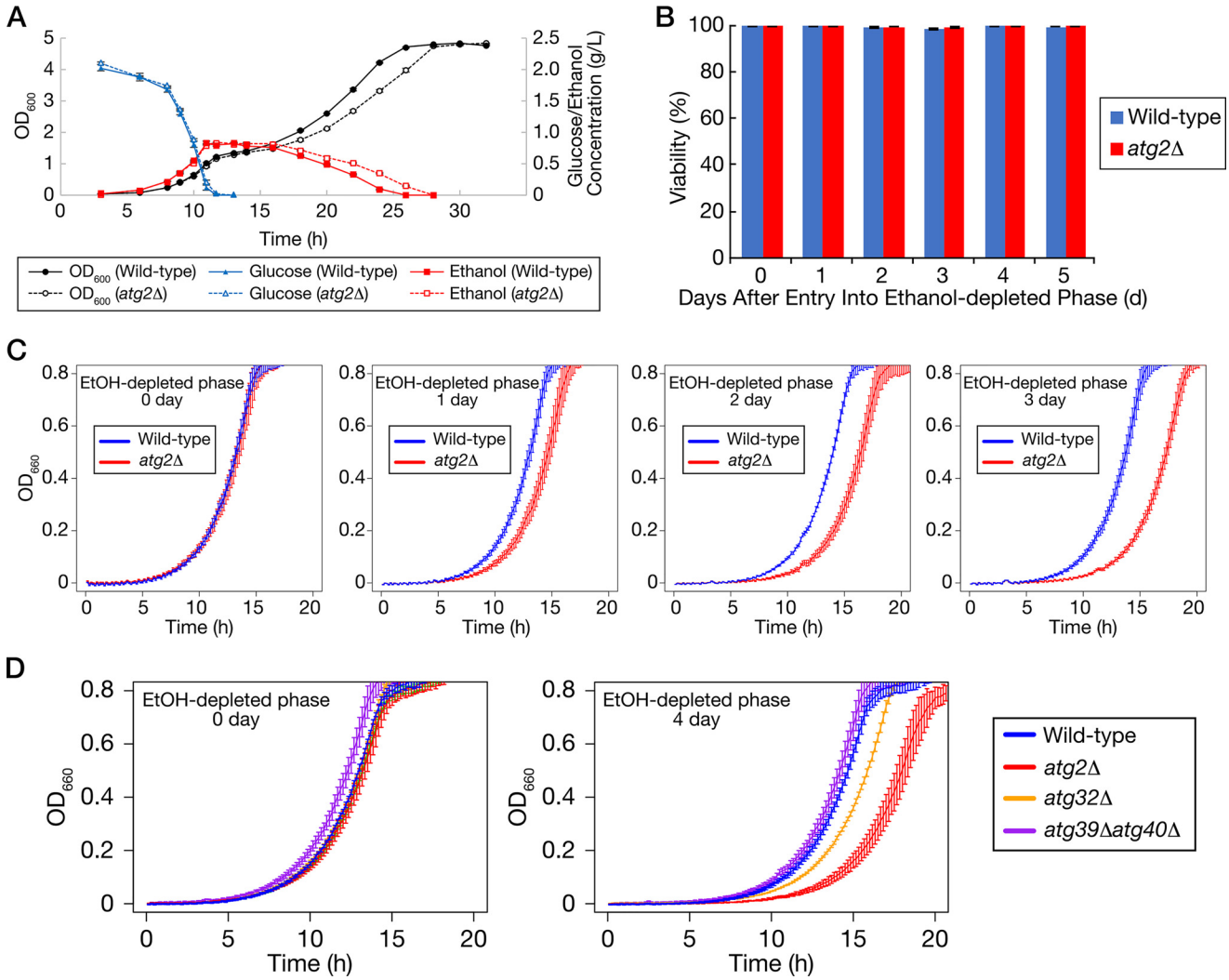

Figure 8. Autophagy-defective cells exhibit slower growth in the ethanol-utilizing phase and delayed re-growth after return to rich medium after ethanol-depleted phase. *A,* WT or *atg2*Δ cells were inoculated into $SD_{0.2}CA$ medium at a starting OD_{600} of 0.01 and cultured for 32 h. OD_{600} (*black circle*), glucose concentration (*blue triangle*), and ethanol concentration (*red square*) in the cultures were measured at the indicated time points. *Filled* and *open symbols* represent the results from the WT and *atg2*Δ strains, respectively. *Data points* and *error bars* represent means ± S.E. ($n = 3$). *B,* WT or *atg2*Δ cells were inoculated into $SD_{0.2}CA$ medium at a starting OD_{600} of 0.01 and cultured for the indicated time periods. Viabilities of these cells were measured. Each result represents an average of calculated viability ± S.E. ($n = 3$). *C,* WT or *atg2*Δ cells were inoculated into $SD_{0.2}CA$ medium at a starting OD_{600} of 0.01 and then cultured for the indicated time periods. The cells were re-inoculated into $SD_{0.2}CA$ medium at a starting OD_{600} of 0.01 and cultured in an automatically recording incubator. The OD_{660} of the culture was measured every 10 min. Each result represents the mean ± S.E. ($n = 3$). *D,* WT, *atg2*Δ, *atg32*Δ, or *atg39*Δ*atg40*Δ cells were inoculated into $SD_{0.2}CA$ medium at a starting OD_{600} of 0.01 and cultured for 0 or 4 days after entry into ethanol-depleted phase. The cells were re-inoculated into $SD_{0.2}CA$ medium at a starting OD_{600} of 0.01 and cultured in an automatically recording incubator. The OD_{660} of the culture was measured every 10 min. Each result represents the mean ± S.E. ($n = 3$).

that bulk autophagy and ER-phagy were induced starting in the ethanol-utilizing phase and that the level of bulk autophagic activity increased in the ethanol-depleted phase (Figs. 3, 4, 6). In contrast, mitophagy occurred only in the ethanol-depleted phase (Figs. 3–6). Induction of autophagy in the ethanol-utilizing phase is an interesting discovery because nutrient availability is expected to be sufficient for yeast growth at this stage. This result implies that autophagy is constitutively induced in the absence of glucose. Consistent with this, our group previously reported that autophagy is induced during the diauxic shift, *i.e.* after glucose depletion, in SD medium (18). In the ethanol-depleted phase, bulk autophagy is more strongly activated, and the mitochondria become targets of autophagy. Thus, we demonstrated that distinct types of autophagy are induced during gradual changes of the carbon source availability.

Our previous report showed that iron levels are insufficient in SD medium after the diauxic shift and that growth after the diauxic shift is not logarithmic (18). Consistent with this, multiple studies have reported nonlogarithmic growth after the diauxic shift (28, 34, 35). Here, we showed that yeast growth was logarithmic in the ethanol-utilizing phase in low-glucose medium (Fig. 1*D*). In standard synthetic medium, certain nutrients are probably not present at sufficient levels for ethanol-utilizing growth. It is noteworthy that some essential nutrients in standard synthetic dextrose medium are insufficient to fully support yeast growth even during glucose-utilizing growth (36). These observations emphasize that the composition of growth media should be carefully considered when we perform long-term cultivation to investigate cellular responses to gradual environmental changes. In particular, the term "stationary

phase" is often used without precise definition. Importantly, under our experimental conditions, stationary phase was caused by ethanol depletion.

In this study, we revealed that three types of macroautophagy are induced after glucose depletion: bulk autophagy, ER-phagy, and mitophagy (Figs. 3, 4, and 6). However, the peroxisome and LDs were not degraded (Fig. 3, *E* and *F*). Rather, both organelles increased during the ethanol-utilizing phase. Because lipases for triacylglycerols and steryl esters are localized in LDs (37–40), fatty acids may be produced via lipolysis in the cytosol, converted to acyl-CoA, and assimilated in the peroxisome, which has β-oxidation activity in yeast, in the ethanol-depleted phase (41). The mitochondria should be needed to produce ATP, but the required amount of the mitochondria may be less in the ethanol-depleted phase than the ethanol-utilizing phase. Hence, the mitochondria may be degraded in the ethanol-depleted phase (Fig. 3*D*). There may be mechanisms so that organelle balance is appropriately adjusted according to the environment surrounding cells, and autophagy may contribute the mechanisms.

Here, we further investigated the dependence of *ATG17* or *ATG11* on those types of autophagy (Fig. 4). It is now accepted that Atg11 functions as a scaffold protein to organize the PAS for selective autophagy. Indeed, ER-phagy induced by rapamycin treatment is partially dependent on *ATG11* (16). Interestingly, under the ethanol-depleted condition, deletion of *ATG11* did not influence ER degradation (Fig. 4*B*). One possible explanation for the weak dependence of ER-phagy on Atg11 in the ethanol-depleted phase is that a large fraction of Atg11 might be preferentially recruited to the mitochondria. It is noteworthy that ER-phagy receptors are still required for ER degradation under these conditions (Fig. 4*B*). In the case of mitophagy, Atg11 plays an essential role (12, 13). Consistent with this, the mitochondria were not degraded in *atg11*Δ cells in ethanol-depleted phase (Fig. 4*C*). Under our experimental conditions, the mitochondria should be well-developed at the starting point of the ethanol-depleted phase, because the cells had previously undergone the ethanol-utilizing phase. To degrade those mitochondria, many molecules of Atg11 might be needed. Detailed observation of the behavior of Atg11 and various organelles under the same conditions will reveal the roles of scaffold proteins, including Atg17. The observation that the mitochondrial degradation is partially dependent on *ATG17* implies that Atg17 functions with Atg11 (Fig. 4*C*). If these two Atg proteins functioned independently, the mitochondria would be degraded in *atg11*Δ cells. Therefore, it is necessary to carefully examine the balance of various autophagy and scaffold protein(s).

Questions remain regarding the effects of autophagy on the intracellular environment. Here, we demonstrated that autophagy-deficient cells exhibited slower growth in the ethanol-utilizing phase (Fig. 8, *A* and *B*). Previously, our group reported that autophagy-defective mutants exhibit a growth defect after the diauxic shift and that autophagy during the diauxic shift in SD medium contributes to iron recycling (18). However, $SD_{0.2}CA$ medium contains enough iron to support respiratory growth (data not shown). Because the proteomic profile changes dynamically during the diauxic shift (35), autophagy induced after glucose depletion might degrade some glycolytic enzymes, which are abundant in glucose-containing medium, thereby causing the yeast to rapidly alter the intracellular proteome in preparation for the ethanol-utilizing phase. Alternatively, amino acids, which are important for ethanol-utilizing growth, may be released by autophagy. We also showed that autophagy in the ethanol-depleted phase was required to promote re-growth in fresh medium (Fig. 8, *C* and *D*). Interestingly, mitophagy was required for the rapid adaptation (Fig. 8*D*). Reactive oxygen species (ROS) accumulate in autophagy-deficient cells under nitrogen starvation (42, 43) and in mitophagy-deficient cells under starvation after respiratory growth (44). It is possible that ROS released from excess mitochondria accumulate in *atg2*Δ or *atg32*Δ cells in ethanol-depleted phase; if so, these ROS could damage cellular components in a way that inhibits rapid adaptation to fresh medium.

The type of microautophagy that involves invagination of the vacuolar membrane, recently named Type 2 microautophagy (4), occurs after the diauxic shift in YEPD medium or standard synthetic complete medium (32, 45). Our results are consistent with those findings: microautophagy occurred in the ethanol-utilizing and ethanol-depleted phases, *i.e.* after diauxic shift. The vacuole invagination process occurs under various conditions, and it results in incorporation of various organelles into the vacuolar lumen (46–49). Although we found that cytosol and LDs are delivered to the vacuolar lumen (Fig. 7, *E* and *F*), it is possible that microautophagy results in uptake of other cellular components. One discrepancy is that Pgk1-GFP was barely cleaved in *atg2*Δ cells, although cleavage of GFP-Atg8 and Vph1-GFP was clearly detected (Figs. 4*A* and 7, *B* and *D*). Moreover, Osw5-GFP was not cleaved in the WT cells despite the presence of LDs in the vacuolar lumen (Fig. 7*F* and Movie S2). In the ethanol-depleted phase, microautophagic bodies containing cytosol and LDs were detected in the vacuolar lumen of WT cells, implying that they were not being efficiently degraded (Fig. 7*E*, *upper panel*). A possible explanation about these discrepancies is that the disintegration speed of microautophagic bodies might differ depending on their contents, resulting in different rates of cleavage. As described above, it is possible that LDs are degraded in the cytosol. It will be an interesting issue to clarify the contribution of LD degradations between in the vacuole and in the cytosol.

Carbon metabolism is a fundamental biological process that is involved in the production of energy and basic cellular components. We should be aware that the metabolic pathways of various nutrients are intricately connected with one another. Here, we focused on carbon source availability, but these influences extend to metabolism of nucleic acids and amino acids, which are deeply involved in induction of autophagy. In the future, integrated metabolomic analyses will provide a better understanding of the physiological roles of autophagy.

Experimental procedures

Yeast strains and growth conditions

Yeast strains used in this study are listed in Table 1. Gene deletions and epitope tagging of genes at endogenous loci were

Table 1
Yeast strains used in this study

Strain	Genotype	Source	Data no.
X2180-1B	*MATα SUC2 mal mel gal2 CUP1*	Yeast genetic stock center	Figs. 1, 6, *A–C*, 7*E*, and 8, Figs. S1 and S2, and Movie S2
RIX47	X2180-1B *atg2Δ::kanMX6*	This study	Fig. 8
RIX151	X2180-1B *atg15Δ::kanMX6*	This study	Fig. 3*H*
RIX175	X2180-1B *atg32Δ::kanMX6*	This study	Fig. 8*D*
RIX525	X2180-1B *atg39Δ::kanMX6 atg40Δ::natNT2*	This study	Fig. 8*D*
RIX471	X2180-1B *atg2Δ::kanMX6 atg15Δ::natNT2*	This study	Fig. 7*E*
MMY98	X2180-1B *atg8::GFP-ATG8::hphNT1*	53	Figs. 2, 6*D*, and 7, *A* and *B*
RIX19	X2180-1B *atg8::GFP-ATG8::hphNT1 atg1Δ::kanMX6*	This study	Fig. 7*A*
MMY104	X2180-1B *atg8::GFP-ATG8::hphNT1 atg2Δ::kanMX6*	53	Figs. 2, 6*D*, and 7, *A* and *B*
RIX67	X2180-1B *atg8::GFP-ATG8::hphNT1 atg3Δ::kanMX6*	This study	Fig. 7*A*
RIX69	X2180-1B *atg8::GFP-ATG8::hphNT1 atg4Δ::kanMX6*	This study	Fig. 7*A*
RIX71	X2180-1B *atg8::GFP-ATG8::hphNT1 atg5Δ::kanMX6*	This study	Fig. 7*A*
RIX73	X2180-1B *atg8::GFP-ATG8::hphNT1 atg6Δ::kanMX6*	This study	Fig. 7*A*
RIX22	X2180-1B *atg8::GFP-ATG8::hphNT1 atg7Δ::kanMX6*	This study	Fig. 7*A*
RIX185	X2180-1B *atg8::GFP-ATG8::hphNT1 atg9Δ::kanMX6*	This study	Fig. 7*A*
RIX75	X2180-1B *atg8::GFP-ATG8::hphNT1 atg10Δ::kanMX6*	This study	Fig. 7*A*
RIX77	X2180-1B *atg8::GFP-ATG8::hphNT1 atg12Δ::kanMX6*	This study	Fig. 7*A*
RIX187	X2180-1B *atg8::GFP-ATG8::hphNT1 atg13Δ::kanMX6*	This study	Fig. 7*A*
RIX189	X2180-1B *atg8::GFP-ATG8::hphNT1 atg14Δ::kanMX6*	This study	Fig. 7*A*
RIX191	X2180-1B *atg8::GFP-ATG8::hphNT1 atg15Δ::kanMX6*	This study	Movie S1
RIX193	X2180-1B *atg8::GFP-ATG8::hphNT1 atg16Δ::kanMX6*	This study	Fig. 7*A*
RIX197	X2180-1B *atg8::GFP-ATG8::hphNT1 atg18Δ::kanMX6*	This study	Fig. 7*A*
RIX587	X2180-1B *atg8::GFP-ATG8::hphNT1 vps4Δ::kanMX6*	This study	Fig. 7*B*
RIX589	X2180-1B *atg8::GFP-ATG8::hphNT1 vps4Δ::kanMX6 atg2Δ::kanMX6*	This study	Fig. 7*B*
RIX113	X2180-1B *atg8::GFP-ATG8::hphNT1 atg2Δ::kanMX6 atg15Δ::natNT2*	This study	Movie S1
TMK834	X2180-1B *pgk1::PGK1-GFP::kanMX4*	19	Figs. 3*B*, 4*A*, and 6*E*
TMK858	X2180-1B *pgk1::PGK1-GFP::kanMX4 atg2Δ::hphNT1*	19	Figs. 4*A* and 6*E*
TMK911	X2180-1B *pgk1::PGK1-GFP::kanMX4 atg11Δ::hphNT1*	This study	Fig. 4*A*
RIX16	X2180-1B *pgk1::PGK1-GFP::kanMX4 atg17Δ::hphNT1*	This study	Fig. 4*A*
RIX179	X2180-1B *sec63::SEC63-GFP::kanMX4*	This study	Figs. 3, *C* and *G*, 4*B*, and 6*F*
RIX493	X2180-1B *sec63::SEC63-GFP::kanMX4 atg2Δ::hphNT1*	This study	Figs. 4*B* and 6*F*
RIX495	X2180-1B *sec63::SEC63-GFP::kanMX4 atg11Δ::hphNT1*	This study	Fig. 4*B*
RIX507	X2180-1B *sec63::SEC63-GFP::kanMX4 atg17Δ::hphNT1*	This study	Fig. 4*B*
RIX497	X2180-1B *sec63::SEC63-GFP::kanMX4 atg39Δ::hphNT1*	This study	Fig. 4*B*
RIX499	X2180-1B *sec63::SEC63-GFP::kanMX4 atg40Δ::hphNT1*	This study	Fig. 4*B*
RIX509	X2180-1B *sec63::SEC63-GFP::kanMX4 atg39Δ::hphNT1 atg40Δ::natNT2*	This study	Fig. 4*B*
RIX183	X2180-1B *om45::OM45-GFP::kanMX4*	This study	Figs. 3, *D* and *G*, 4*C*, 5*B*, and 6*G*
RIX293	X2180-1B *om45::OM45-GFP::kanMX4 atg2Δ::hphNT1*	This study	Figs. 4*C* and 6*G*
RIX483	X2180-1B *om45::OM45-GFP::kanMX4 atg11Δ::hphNT1*	This study	Fig. 4*C*
RIX485	X2180-1B *om45::OM45-GFP::kanMX4 atg17Δ::hphNT1*	This study	Fig. 4*C*
RIX307	X2180-1B *om45::OM45-GFP::kanMX4 atg32Δ::hphNT1*	This study	Fig. 4*C*
RIX181	X2180-1B *pex11::PEX11-GFP::kanMX4*	This study	Fig. 3*E*
RIX511	X2180-1B *osw5::OSW5-GFP::kanMX4*	This study	Fig. 3*F*
RIX345	X2180-1B *vph1::VPH1-GFP::kanMX4*	This study	Fig. 7, *C* and *D*
RIX349	X2180-1B *vph1::VPH1-GFP::kanMX4 atg1Δ::hphNT1*	This study	Fig. 7*C*
RIX351	X2180-1B *vph1::VPH1-GFP::kanMX4 atg2Δ::hphNT1*	This study	Fig. 7*C*
RIX353	X2180-1B *vph1::VPH1-GFP::kanMX4 atg7Δ::hphNT1*	This study	Fig. 7*C*
RIX355	X2180-1B *vph1::VPH1-GFP::kanMX4 atg8Δ::hphNT1*	This study	Fig. 7*C*
RIX359	X2180-1B *vph1::VPH1-GFP::kanMX4 atg14Δ::hphNT1*	This study	Fig. 7*C*
RIX501	X2180-1B *vph1::VPH1-GFP::kanMX4 vps4Δ::hphNT1*	This study	Fig. 7*C*
RIX389	X2180-1B *vph1::VPH1-mCherry::hphNT1*	This study	Fig. 7*F*

performed by PCR-based methods and validated by PCR (50, 51).

An appropriate carbon source was added to YNB medium (1 g/liter potassium dihydrogen phosphate, 0.5 g/liter magnesium sulfate heptahydrate, 0.1 g/liter sodium chloride, 0.1 g/liter calcium chloride dihydrate, 2 mg/liter *myo*-inositol, 0.4 mg/liter calcium (+)-pantothenate, 0.4 mg/liter nicotinic acid, 0.4 mg/liter pyridoxine hydrochloride, 0.4 mg/liter thiamine hydrochloride, 0.2 mg/liter *p*-aminobenzoic acid, 0.2 mg/ml riboflavin, 2 μg/liter (+)-biotin, 2 μg/liter folic acid, 0.5 mg/ml boric acid, 0.4 mg/liter manganese(II) sulfate pentahydrate, 0.4 mg/liter zinc sulfate heptahydrate, 0.2 mg/liter iron(III) chloride hexahydrate, 0.2 mg/liter disodium molybdate(VI) dihydrate, 0.1 mg/liter potassium iodide, 0.04 mg/liter copper(II) sulfate pentahydrate, 5 g/liter ammonium sulfate) containing 0.5% Bacto™ casamino acid (Difco), as follows: 2% (w/v) glucose (SDCA medium) or 0.2% (w/v) glucose ($SD_{0.2}$CA medium). To prepare $SD_{0.2}$ medium, 0.2%(w/v) glucose was added to YNB medium.

Yeast cells were inoculated from YPD plates (1% Bacto™ yeast extract (Difco), 2% Bacto™ peptone (Difco), 2% glucose, 2% agar) into 2 ml of SDCA medium in a test tube and grown overnight (pre-culture) at 30 °C and 187 rpm using a rotator (RT-550, TAITEC Corp.) until glucose was completely exhausted. These cells were inoculated into fresh medium and cultured under the indicated conditions. Unless otherwise mentioned, yeast cells were grown at 30 °C and 180 rpm in a 125-ml Erlenmeyer baffled flask (Corning) on a BioShaker (BR-43FL, TAITEC Corp.).

Growth curve analyses

OD_{600} of yeast cultures were obtained using a spectrometer (U-2900, Hitachi) at the indicated time points after cultures were diluted to appropriate concentrations. For automatic

growth curve analyses, pre-cultured cells were inoculated at a starting OD_{600} of 0.01 into 5 ml of the indicated medium in L-shaped tubes and then cultured at 30 °C at 60 rpm in an automatically recording incubator (TVS062CA, Advantec). OD_{660} of yeast cultures was recorded every 10 min. Growth curves were obtained by connecting the average values of the respective times ($n = 3$).

Measurement of dry cell weight

Yeast cells were collected by centrifugation (10,000 rpm, 1 min), washed with distilled water, and collected by centrifugation (10,000 rpm, 1 min). The supernatant was discarded; the resultant pellet was frozen by liquid nitrogen, and the frozen-pellet was freeze-dried overnight using a freeze dryer (VD-500F, TAITEC Corp.). Weight of the dried yeast cells was measured, and the dry cell weight per 1-liter of culture was calculated.

Quantification of glucose and ethanol concentration in cultures

Medium or yeast cultures were centrifuged at 10,000 rpm for 1 min, and supernatants were collected. Supernatants were diluted to the appropriate concentrations. Glucose, ethanol, or ammonium concentrations in supernatants were measured using the F-kit D-glucose (JK International Inc.), F-kit ethanol (JK International), or F-kit ammonia (JK International), respectively.

Measurement of oxygen consumption rate

Respiration of yeast cells was measured noninvasively at room temperature using a Fibox3 oxygen meter (PreSens Precision Sensing GmbH) with continuous stirring. Cells were collected and resuspended in 3 ml of YNB medium containing 0.5% (w/v) casamino acids and 1% (v/v) ethanol in a 15-ml tube at appropriate density. Then, the tube was vortexed for 3 s, and the cell suspension was immediately transferred into a cuvette. Dissolved oxygen in the culture was measured every second, with stirring, by the Fibox3. The changes of dissolved oxygen (DO) in the solution per unit time and OD_{600} were calculated ($\Delta DO^{\text{no treatment}}$ (% O_2/OD_{600}/min)) using dissolved oxygen values from 61 to 120 s. The same procedures were performed in the presence of antimycin A (5 μM) or FCCP (10 μM). On the bases of these measurements, $\Delta DO^{\text{antimycin A}}$ and ΔDO^{FCCP} were calculated. Finally, the true values of dissolved oxygen change as $\Delta DO^{\text{no treatment}} - \Delta DO^{\text{antimycin A}}$ (no treatment) or $\Delta DO^{\text{FCCP}} - \Delta DO^{\text{antimycin A}}$ (FCCP) were calculated.

Immunoblot analyses

Immunoblot analyses were performed as described previously (20). Antibodies against GFP (Roche Applied Science), Pgk1 (Invitrogen), β-tubulin (Wako), and Ape1 (a laboratory stock) were used to detect relevant proteins. Chemiluminescence signals were detected using a CCD camera system (LAS4000, GE Healthcare, or Fusion FX, Vilber Lourmat). Quantification of each band intensity was performed using Fusion© software (Vilber Lourmat).

Microscopic image acquisition

Fluorescence microscopy was performed as described previously (20).

Ultrastructural analyses

Ultrastructural analysis of yeast cells was performed by Tokai-EMA (Japan).

BODIPY staining

BODIPY 493/503 was dissolved in DMSO at a final concentration of 1 mg/ml (BODIPY stock solution). Five microliters of the BODIPY stock was added to 495 μl of yeast culture, and the mixture was incubated for 5 min at room temperature.

Determination of cell viability

Cell viability was determined by phloxine B staining (52). Phloxine B was added to yeast cultures at a final concentration of 2.5 μg/ml. Cells were observed using an inverted fluorescence microscope (IX81, Olympus) equipped with a cooled CCD camera (CoolSNAP HQ, Photometrics) and a ×40 objective lens (Uplan Apo ×40, Olympus) at room temperature. A power supply (BH2-RFL-T3, Olympus) was used to excite phloxine B. To obtain phloxine B fluorescence, an excitation filter (BP535-555HQ, Olympus), a dichroic filter (DM565HQ, Olympus), and a fluorescence filter (BA570-625HQ, Olympus) were used. Images were acquired using the MetaMorph software (Molecular Devices).

Author contributions—R. I. conceptualization; R. I. data curation; R. I. formal analysis; R. I. validation; R. I. and Y. O. investigation; R. I. writing-original draft; Y. O. supervision; Y. O. project administration; Y. O. writing-review and editing.

Acknowledgments—We are grateful to members of the Ohsumi laboratory for helpful discussion. We thank Dr. Alexander May for useful discussion, and Mizuki Morishita for excellent assistance with experiments.

References

1. Nakatogawa, H., Suzuki, K., Kamada, Y., and Ohsumi, Y. (2009) Dynamics and diversity in autophagy mechanisms: lessons from yeast. *Nat. Rev. Mol. Cell Biol.* **10,** 458–467 CrossRef Medline
2. Gatica, D., Lahiri, V., and Klionsky, D. J. (2018) Cargo recognition and degradation by selective autophagy. *Nat. Cell Biol.* **20,** 233–242 CrossRef Medline
3. Mizushima, N., and Komatsu, M. (2011) Autophagy: renovation of cells and tissues. *Cell* **147,** 728–741 CrossRef Medline
4. Oku, M., and Sakai, Y. (2018) Three distinct types of microautophagy based on membrane dynamics and molecular machineries. *Bioessays* **40,** e1800008 Medline
5. Noda, N. N., and Inagaki, F. (2015) Mechanisms of autophagy. *Annu. Rev. Biophys.* **44,** 101–122 CrossRef Medline
6. Suzuki, K., Kirisako, T., Kamada, Y., Mizushima, N., Noda, T., and Ohsumi, Y. (2001) The pre-autophagosomal structure organized by concerted functions of *APG* genes is essential for autophagosome formation. *EMBO J.* **20,** 5971–5981 CrossRef Medline
7. Suzuki, K., Kubota, Y., Sekito, T., and Ohsumi, Y. (2007) Hierarchy of Atg proteins in pre-autophagosomal structure organization. *Genes Cells* **12,** 209–218 CrossRef Medline
8. Suzuki, K. (2013) Selective autophagy in budding yeast. *Cell Death. Differ.* **20,** 43–48 CrossRef Medline

9. Kim, J., Kamada, Y., Stromhaug, P. E., Guan, J., Hefner-Gravink, A., Baba, M., Scott, S. V., Ohsumi, Y., Dunn, W. A., Jr., and Klionsky, D. J. (2001) Cvt9/Gsa9 functions in sequestering selective cytosolic cargo destined for the vacuole. *J. Cell Biol.* **153,** 381–396 CrossRef Medline
10. Scott, S. V., Guan, J., Hutchins, M. U., Kim, J., and Klionsky, D. J. (2001) Cvt19 is a receptor for the cytoplasm-to-vacuole targeting pathway. *Mol. Cell* **7,** 1131–1141 CrossRef Medline
11. Suzuki, K., Kondo, C., Morimoto, M., and Ohsumi, Y. (2010) Selective transport of α-mannosidase by autophagic pathways: identification of a novel receptor, Atg34p. *J. Biol. Chem.* **285,** 30019–30025 CrossRef Medline
12. Okamoto, K., Kondo-Okamoto, N., and Ohsumi, Y. (2009) Mitochondria-anchored receptor Atg32 mediates degradation of mitochondria via selective autophagy. *Dev. Cell* **17,** 87–97 CrossRef Medline
13. Kanki, T., Wang, K., Cao, Y., Baba, M., and Klionsky, D. J. (2009) Atg32 is a mitochondrial protein that confers selectivity during mitophagy. *Dev. Cell* **17,** 98–109 CrossRef Medline
14. Farré, J. C., Manjithaya, R., Mathewson, R. D., and Subramani, S. (2008) PpAtg30 tags peroxisomes for turnover by selective autophagy. *Dev. Cell* **14,** 365–376 CrossRef Medline
15. Motley, A. M., Nuttall, J. M., and Hettema, E. H. (2012) Pex3-anchored Atg36 tags peroxisomes for degradation in *Saccharomyces cerevisiae*. *EMBO J.* **31,** 2852–2868 CrossRef Medline
16. Mochida, K., Oikawa, Y., Kimura, Y., Kirisako, H., Hirano, H., Ohsumi, Y., and Nakatogawa, H. (2015) Receptor-mediated selective autophagy degrades the endoplasmic reticulum and the nucleus. *Nature* **522,** 359–362 CrossRef Medline
17. Onodera, J., and Ohsumi, Y. (2005) Autophagy is required for maintenance of amino acid levels and protein synthesis under nitrogen starvation. *J. Biol. Chem.* **280,** 31582–31586 CrossRef Medline
18. Horie, T., Kawamata, T., Matsunami, M., and Ohsumi, Y. (2017) Recycling of iron via autophagy is critical for the transition from glycolytic to respiratory growth. *J. Biol. Chem.* **292,** 8533–8543 CrossRef Medline
19. Kawamata, T., Horie, T., Matsunami, M., Sasaki, M., and Ohsumi, Y. (2017) Zinc starvation induces autophagy in yeast. *J. Biol. Chem.* **292,** 8520–8530 CrossRef Medline
20. Adachi, A., Koizumi, M., and Ohsumi, Y. (2017) Autophagy induction under carbon starvation conditions is negatively regulated by carbon catabolite repression. *J. Biol. Chem.* **292,** 19905–19918 CrossRef Medline
21. Yokota, H., Gomi, K., and Shintani, T. (2017) Induction of autophagy by phosphate starvation in an Atg11-dependent manner in *Saccharomyces cerevisiae*. *Biochem. Biophys. Res. Commun.* **483,** 522–527 CrossRef Medline
22. Frankel, D. G. (2011) *Yeast Intermediary Metabolism*, Cold Spring Harbor Laboratory Press, Cold Spring Harbor, NY
23. Fiechter, A., Fuhrmann, G. F., and Käppeli, O. (1981) Regulation of glucose metabolism in growing yeast cells. *Adv. Microb. Physiol.* **22,** 123–183 CrossRef Medline
24. van Dijken, J. P., Weusthuis, R. A., and Pronk, J. T. (1993) Kinetics of growth and sugar consumption in yeasts. *Antonie Van Leeuwenhoek* **63,** 343–352 CrossRef Medline
25. Dickinson, J. R., and Schweizer, M. (1999) *The Metabolism and Molecular Physiology of Saccharomyces cerevisiae*. Taylor & Francis, Inc., Philadelphia, PA
26. Kayikci Ö., and Nielsen, J. (2015) Glucose repression in *Saccharomyces cerevisiae*. *FEMS Yeast Res.* **15,** fov068 CrossRef Medline
27. Ohlmeier, S., Kastaniotis, A. J., Hiltunen, J. K., and Bergmann, U. (2004) The yeast mitochondrial proteome, a study of fermentative and respiratory growth. *J. Biol. Chem.* **279,** 3956–3979 CrossRef Medline
28. Stahl, G., Salem, S. N., Chen, L., Zhao, B., and Farabaugh, P. J. (2004) Translational accuracy during exponential, postdiauxic, and stationary growth phases in *Saccharomyces cerevisiae*. *Eukaryot. Cell* **3,** 331–338 CrossRef Medline
29. Cheong, H., and Klionsky, D. J. (2008) Biochemical methods to monitor autophagy-related processes in yeast. *Methods Enzymol.* **451,** 1–26 CrossRef Medline
30. Teter, S. A., Eggerton, K. P., Scott, S. V., Kim, J., Fischer, A. M., and Klionsky, D. J. (2001) Degradation of lipid vesicles in the yeast vacuole requires function of Cvt17, a putative lipase. *J. Biol. Chem.* **276,** 2083–2087 CrossRef Medline
31. Fukuda, T., and Kanki, T. (2018) Mechanisms and physiological roles of mitophagy in yeast. *Mol. Cells* **41,** 35–44 Medline
32. Oku, M., Maeda, Y., Kagohashi, Y., Kondo, T., Yamada, M., Fujimoto, T., and Sakai, Y. (2017) Evidence for ESCRT- and clathrin-dependent microautophagy. *J. Cell Biol.* **216,** 3263–3274 CrossRef Medline
33. Piper, R. C., and Katzmann, D. J. (2007) Biogenesis and function of multivesicular bodies. *Annu. Rev. Cell Dev. Biol.* **23,** 519–547 CrossRef Medline
34. Haurie, V., Boucherie, H., and Sagliocco, F. (2003) The Snf1 protein kinase controls the induction of genes of the iron uptake pathway at the diauxic shift in *Saccharomyces cerevisiae*. *J. Biol. Chem.* **278,** 45391–45396 CrossRef Medline
35. Murphy, J. P., Stepanova, E., Everley, R. A., Paulo, J. A., and Gygi, S. P. (2015) Comprehensive temporal protein dynamics during the diauxic shift in *Saccharomyces cerevisiae*. *Mol. Cell. Proteomics* **14,** 2454–2465 CrossRef Medline
36. Hanscho, M., Ruckerbauer, D. E., Chauhan, N., Hofbauer, H. F., Krahulec, S., Nidetzky, B., Kohlwein, S. D., Zanghellini, J., and Natter, K. (2012) Nutritional requirements of the BY series of *Saccharomyces cerevisiae* strains for optimum growth. *FEMS Yeast Res.* **12,** 796–808 CrossRef Medline
37. Athenstaedt, K., and Daum, G. (2003) *YMR313c/TGL3* encodes a novel triacylglycerol lipase located in lipid particles of *Saccharomyces cerevisiae*. *J. Biol. Chem.* **278,** 23317–23323 CrossRef Medline
38. Athenstaedt, K., and Daum, G. (2005) Tgl4p and Tgl5p, two triacylglycerol lipases of the yeast *Saccharomyces cerevisiae* are localized to lipid particles. *J. Biol. Chem.* **280,** 37301–37309 CrossRef Medline
39. Köffel, R., Tiwari, R., Falquet, L., and Schneiter, R. (2005) The *Saccharomyces cerevisiae YLL012/YEH1*, *YLR020/YEH2*, and *TGL1* genes encode a novel family of membrane-anchored lipases that are required for steryl ester hydrolysis. *Mol. Cell. Biol.* **25,** 1655–1668 CrossRef Medline
40. Ploier, B., Scharwey, M., Koch, B., Schmidt, C., Schatte, J., Rechberger, G., Kollroser, M., Hermetter, A., and Daum, G. (2013) Screening for hydrolytic enzymes reveals Ayr1p as a novel triacylglycerol lipase in *Saccharomyces cerevisiae*. *J. Biol. Chem.* **288,** 36061–36072 CrossRef Medline
41. Sibirny, A. A. (2016) Yeast peroxisomes: structure, functions and biotechnological opportunities. *FEMS Yeast Res.* **16,** fow038 Medline
42. Suzuki, S. W., Onodera, J., and Ohsumi, Y. (2011) Starvation induced cell death in autophagy-defective yeast mutants is caused by mitochondria dysfunction. *PLoS ONE* **6,** e17412 CrossRef Medline
43. Medeiros, T. C., Thomas, R. L., Ghillebert, R., and Graef, M. (2018) Autophagy balances mtDNA synthesis and degradation by DNA polymerase POLG during starvation. *J. Cell Biol.* **217,** 1601–1611 CrossRef Medline
44. Kurihara, Y., Kanki, T., Aoki, Y., Hirota, Y., Saigusa, T., Uchiumi, T., and Kang, D. (2012) Mitophagy plays an essential role in reducing mitochondrial production of reactive oxygen species and mutation of mitochondrial DNA by maintaining mitochondrial quantity and quality in yeast. *J. Biol. Chem.* **287,** 3265–3272 CrossRef Medline
45. Tsuji, T., Fujimoto, M., Tatematsu, T., Cheng, J., Orii, M., Takatori, S., and Fujimoto, T. (2017) Niemann-Pick type C proteins promote microautophagy by expanding raft-like membrane domains in the yeast vacuole. *Elife* **6,** e25960 CrossRef Medline
46. Moeller, C. H., and Thomson, W. W. (1979) Uptake of lipid bodies by the yeast vacuole involving areas of the tonoplast depleted of intramembranous particles. *J. Ultrastruct. Res.* **68,** 38–45 CrossRef Medline
47. Müller, O., Sattler, T., Flötenmeyer, M., Schwarz, H., Plattner, H., and Mayer, A. (2000) Autophagic tubes: vacuolar invaginations involved in lateral membrane sorting and inverse vesicle budding. *J. Cell Biol.* **151,** 519–528 CrossRef Medline
48. Kissová, I., Salin, B., Schaeffer, J., Bhatia, S., Manon, S., and Camougrand, N. (2007) Selective and non-selective autophagic degradation of mitochondria in yeast. *Autophagy* **3,** 329–336 CrossRef Medline
49. Roberts, P., Moshitch-Moshkovitz, S., Kvam, E., O'Toole, E., Winey, M., and Goldfarb, D. S. (2003) Piecemeal microautophagy of nucleus in *Saccharomyces cerevisiae*. *Mol. Biol. Cell* **14,** 129–141 CrossRef Medline

50. Knop, M., Siegers, K., Pereira, G., Zachariae, W., Winsor, B., Nasmyth, K., and Schiebel, E. (1999) Epitope tagging of yeast genes using a PCR-based strategy: more tags and improved practical routines. *Yeast* **15,** 963–972 CrossRef Medline
51. Janke, C., Magiera, M. M., Rathfelder, N., Taxis, C., Reber, S., Maekawa, H., Moreno-Borchart, A., Doenges, G., Schwob, E., Schiebel, E., and Knop, M. (2004) A versatile toolbox for PCR-based tagging of yeast genes: new fluorescent proteins, more markers and promoter substitution cassettes. *Yeast* **21,** 947–962 CrossRef Medline
52. Noda, T. (2008) Viability assays to monitor yeast autophagy. *Methods Enzymol.* **451,** 27–32 CrossRef Medline
53. Huang, H., Kawamata, T., Horie, T., Tsugawa, H., Nakayama, Y., Ohsumi, Y., and Fukusaki, E. (2015) Bulk RNA degradation by nitrogen starvation-induced autophagy in yeast. *EMBO J.* **34,** 154–168 CrossRef Medline